NASA TECHNICAL MEMORANDUM 107575

CLOSED-FORM ANALYSIS OF FIBER-MATRIX INTERFACE STRESSES UNDER THERMO-MECHANICAL LOADINGS

Rajiv A. Naik and John H. Crews, Jr.

March 1992

Presented at the ASTM 11th Symposium on Composite Materials: Testing and Design; Pittsburgh, PA; May 4-5, 1992

National Aeronautics and
Space Administration

Langley Research Center
Hampton, Virginia 23665

ABSTRACT

Closed-form techniques for calculating fiber-matrix (FM) interface stresses, using repeating square and diamond regular arrays, were presented for a unidirectional composite under thermo-mechanical loadings. An Airy's stress function micromechanics approach from the literature, developed for calculating overall composite moduli, was extended in the present study to compute FM interface stresses for a unidirectional graphite/epoxy (AS4/3501-6) composite under thermal, longitudinal, transverse, transverse shear and longitudinal shear loadings. Comparisons with finite element results indicated excellent agreement of the FM interface stresses for the square array. Under thermal and longitudinal loading, the square array had the same FM peak stresses as the diamond array. The square array predicted higher stress concentrations under transverse normal and longitudinal shear loadings than the diamond array. Under transverse shear loading, the square array had a higher shear stress concentration while the diamond array had a higher radial stress concentration. Stress concentration factors under transverse shear and longitudinal shear loadings were very sensitive to fiber volume fraction. The present analysis provides a simple way to calculate accurate FM interface stresses for both the square and diamond array configurations.

Key Words: Repeating unit cell, square array, diamond array, micromechanics, composite.

NOMENCLATURE

a	fiber radius
A_o, B_o, C_o, D_o	arbitrary constants in stress function F
A_n, B_n, C_n, D_n	arbitrary constants in stress function F; n = 2, 4, 6, ...
b	length of one side for square array
C_{ij}	components of stiffness matrix, i=1-3, j=1-3
E	Young's modulus
F	Airy's stress function
G	shear modulus
K_{rr}	normalized peak radial stress under transverse loading
$K_{r\theta}$	normalized peak shear stress under transverse shear loading
K_{rz}	normalized peak shear stress under longitudinal shear loading
r, θ, z	cylindrical cordinates
r_1, θ_1, z	cylindrical coordinate system with origin at H in diamond array
r_2, ϕ_2, z	cylindrical cordinate system with origin at F in diamond array
S_{ij}	components of compliance matrix, i=1-3, j=1-3
$S_{r\theta}$	components of compliance matrix in cylindrical coordinates
T_I, T_F	initial and final temperatures, respectively
u, v, w	displacements in the x, y, and z directions, respectively
V_f	fiber volume fraction
x, y, z	cartesian coordinates
α_r, α_θ, α_z	coefficients of thermal expansion in cylindrical coordinates
α_x, α_y, α_z	coefficients of thermal expansion in cartesian coordinates
ΔT	change in temperature
ε_r, ε_θ, ε_z	normal strains in cylindrical coordinates
ε_{xo}, ε_{yo}, ε_{zo}	applied normal strains in the x, y, and z directions, respectively

$\gamma_{r\theta}$, $\gamma_{\theta z}$, γ_{rz}	shear strains in cylindrical coordinates
γ_{xyo}, γ_{yzo}, γ_{xzo}	applied shear strains in cartesian coordinates
$\eta-\zeta$	cartesian axes rotated by 45 degrees with respect to the x-y axes
ν	Poisson's ratio
σ_r, σ_θ, σ_z	normal stresses in cylindrical coordinates
$\bar{\sigma}_x$, $\bar{\sigma}_y$, $\bar{\sigma}_z$	average normal stresses in the x, y, and z directions, respectively
$\tau_{r\theta}$, $\tau_{\theta z}$, τ_{rz}	shear stresses in cylindrical coordinates
$\bar{\tau}_{xy}$, $\bar{\tau}_{yz}$, $\bar{\tau}_{xz}$	average shear stresses in cartesian coordinates

Superscripts and subscripts

f, m	refer to the fiber and matrix, respectively

INTRODUCTION

The fracture of polymer matrix composites can involve three types of local failures: fiber fracture, matrix cracking, and fiber-matrix (FM) interfacial fracture. While the properties of the fiber and the matrix are important factors, the strength of the FM interface is critical to the failure process and overall composite strength [1]. It is therefore important to characterize FM interface strength. Accurate calculations of FM interface stresses are required to measure FM interface strength and to predict FM interface cracking.

Micromechanical models for unidirectional composites based on both closed-form and numerical approaches have been used extensively in the past. A comprehensive review of earlier micromechanical models is given in reference 2. The simplest and most commonly used is the composite cylinder model [3], which assumes a fiber embedded in a cylindrical matrix. Although it lends itself to a closed-form analysis, this model neglects fiber interactions and, therefore, works well only for low fiber volume fractions. The effect of neighboring fibers has been accounted for by assuming a regular, periodic arrangement of fibers in the composite. FM interface stresses were computed by Foye [4] in 1966, using square and hexagonal periodic arrays and the finite element method. During the same period,

Adams and Doner [5] used a square array and the finite difference method to compute FM interface stresses. More recently, the finite element technique has been used to compute FM interface stresses [6]. The boundary element technique has also been used in a recent study [7].

Numerical solutions usually involve tedious mesh generation and convergence studies and also require large amounts of computing time. Thus, closed-form solutions, which can be programmed on a personal computer, are preferable to numerical ones. In 1974, Kobayashi and Ishikawa [8-10] developed analytical solutions using an Airy's stress function approach for square, diamond, and hexagonal arrays to compute overall thermoelastic constants. Boundary conditions for different loading conditions were satisfied by a point-matching technique. However, they did not provide techniques for computing FM interface stresses. More recently, Averill and Carman [11] developed a similar series-type solution using point-matching along the boundaries for a hexagonal array and computed overall composite properties and FM stresses for different properties of the interphase region between the fiber and the matrix.

Within a composite ply, fibers are arranged randomly and may resemble a square array in some regions, a diamond array in some regions and a hexagonal array in other regions. To characterize FM interface strength and predict FM interface cracking, it is important to use the array that leads to the most critical FM interface stresses under a given loading condition. For a given fiber volume fraction, Foye [4] demonstrated that the stress concentrations at the FM interface, for both normal and shear loadings, are higher for the square array than for the hexagonal array. This may be explained by the fact that the fibers are closer to one another in the square array. Furthermore, for shear loading, the diamond array may have a higher stress concentration than the square array. Therefore, under combined loading, the most critical FM interface stresses will either be produced by the square array or the diamond array. Thus, to characterize the FM interface strength, FM interface stresses calculated using the square and

diamond arrays will need to be compared to determine which array leads to the more critical stresses at the FM interface.

The objective of the present study was to apply closed-form micromechanical techniques to compute accurate FM interface stresses for thermo-mechanical loadings using square and diamond regular arrays. The Airy's stress function approach used by Kobayashi and Ishikawa [9] was adopted in the present analysis for the solution of the basic equations. Procedures for calculating FM interface stresses under thermal, longitudinal, transverse, transverse shear and longitudinal shear loadings were developed in this study. Unit load solutions are presented for each of these load cases. The FM interface stresses computed using the closed-form approach were evaluated using finite element results for the square array. Comparisons were also made between the FM interface stresses calculated using the square and diamond array solutions. Finally, the effects of fiber volume fraction on FM interface stresses are presented.

ANALYTICAL METHODS

As mentioned earlier, the analytical methods used here are based on those presented in References 8-10. However, the emphasis in References 8-10 was on determining overall elastic constants. The procedures for applying various loadings to the models in order to calculate FM interface stresses were developed in the present study. For this micromechanics analysis, these loadings correspond to ply stresses in a laminated composite. Since the basic assumptions in the present study are the same as those in References 8-10, only an outline of the analytical procedures is described here.

Closed-Form Solution

As shown in Fig. 1, the origin of the cylindrical cordinate system used in this study is located at the center of the fiber and the z-direction is along the fiber axis. The fibers are assumed to be circular in cross-section (radius = a), homogeneous, and orthotropic with transverse isotropy in the x-y plane. The matrix is homogeneous and isotropic and the fiber

and matrix are perfectly bonded. A state of generalized plane strain is assumed (ε_z = constant) for all loading cases except the longitudinal shear loading case. Note that the diamond array (Fig. 1(b)) is equivalent to the square array (Fig. 1(a)) rotated by 45 degrees. The analysis uses the repeating unit cell ABCD for the square array, and EGH for the diamond array as indicated by the shaded areas.

The boundary conditions on side EG of the diamond array can be conveniently described by considering three coordinate systems. The polar coordinate system r_1-θ_1 has its origin at H with θ_1 measured with respect to the x-axis. The r_2-ϕ_2 system has its origin at F with ϕ_2 measured with respect to the horizontal x-axis. The angle θ_2 is measured with respect to the line FG. Points along the line AC are shared by the diamonds 1 and 2 which are centered at points H and F, respectively. Thus, a point with coordinates (r_1, θ_1) can also be described by coordinates (r_2, ϕ_2) or by (r_2, θ_2). The cartesian coordinate system $\eta-\zeta$ is rotated by 45 degrees with respect to the x-y coordinate system.

Governing Equation

The present problem can be separated into two cases; (a) all loadings except longitudinal shear (i.e., thermal, longitudinal, transverse, and transverse shear) and (b) longitudinal shear loading. Case (a) can be solved by assuming a state of generalized plane strain which reduces the problem to two dimensions. The Airy's stress function, F, can be used to solve this two-dimensional elasticity problem. The governing biharmonic equation can be written as

$$\nabla^4 F = 0, \qquad \nabla^2 = \frac{\partial^2}{\partial r^2} + \frac{1}{r}\frac{\partial}{\partial r} + \frac{1}{r^2}\frac{\partial^2}{\partial \theta^2} \tag{1}$$

When only average normal stresses, $\bar{\sigma}_x$, $\bar{\sigma}_y$ and $\bar{\sigma}_z$ ($\bar{\tau}_{xy} = 0$) are applied to the composite, the x- and y-axes become axes of symmetry and a general solution to Eq. (1) in the form of a Fourier series can be written as

$$F = F_0(r) + \sum_{n=2,\,even}^{\infty} F_n(r) \cos n\theta,$$

where, (2)

$$F_0(r) = A_0 r^2 + B_0 + C_0 r^2 \log r + D_0 \log r$$

$$F_n(r) = A_n r^{n+2} + B_n r^n + C_n r^{-n+2} + D_n r^{-n}$$

where A_0, B_0, C_0, D_0 and A_n, B_n, C_n and D_n (n = 2, 4, 6, ...) are arbitrary constants. Equation (2) is valid for both the square and diamond arrays only when symmetric loading is applied. Transverse shear loading for both the square and diamond arrays will need special consideration as described later. Case (b), with longitudinal shear loading, will need a different stress function and is described in a later section. The arbitrary coefficients in Eq. (2) are determined by satisfying stress and displacement boundary conditions for each loading. The fiber and matrix regions will each have a different set of arbitrary coefficients.

The expressions for the stress components σ_r, σ_θ, and $\tau_{r\theta}$ can be determined from the stress function F by taking derivatives [8]. The strain components can be expressed in terms of the arbitrary coefficients in Eq. (2) by using the constitutive law. It is assumed that the composite material is transversely isotropic and the constitutive law can be written in cylindrical coordinates as [8,12]

$$\{\varepsilon\} = [S_{r\theta}]\{\sigma\} + \{\alpha\}\Delta T \tag{3}$$

where,

$\{\varepsilon\} = \{\varepsilon_r, \varepsilon_\theta, \varepsilon_z, \gamma_{r\theta}, \gamma_{\theta z}, \gamma_{rz}\}$,

$\{\sigma\} = \{\sigma_r, \sigma_\theta, \sigma_z, \tau_{r\theta}, \tau_{\theta z}, \tau_{rz}\}$,

$\{\alpha\} = \{\alpha_r, \alpha_\theta, \alpha_z, 0, 0, 0\}$ coefficients of thermal expansion,

$[S_{r\theta}]$ = compliance matrix (in cylindrical coordinates),

and $\Delta T = T_F - T_I$ = temperature change.

The expressions for the displacements u_r and u_θ can then be obtained by integrating the expressions for the normal strains [8,10]. Note that for the thermal loading case, temperature dependent material properties can be readily incorporated into the analysis by considering an incremental form for Eq. (3), in which $\{\varepsilon\}$, $\{\sigma\}$, and ΔT are replaced by $\{\delta\varepsilon\}$, $\{\delta\sigma\}$, and δT, respectively, and following the incremental procedure outlined in Ref. 10. The effects of moisture can also be readily incorporated into the analysis by adding to Eq. (3) an extra term which is similar to the thermal strain term with the coefficients of thermal expansion replaced by the coefficients of moisture absorption.

Internal Boundary Conditions

Using the expressions for the stresses and displacements, the internal boundary conditions at the fiber-matrix interface for both the square and the diamond array can be written as,

$$\begin{aligned} (\sigma_r)_f &= (\sigma_r)_m, \quad (\tau_{r\theta})_f = (\tau_{r\theta})_m, \\ (u_r)_f &= (u_r)_m, \quad (u_\theta)_f = (u_\theta)_m. \end{aligned} \tag{4}$$

where the subscripts f and m correspond to the fiber and matrix, respectively. As explained in Ref. 8, the coefficients of the inverse powers associated with the fibers, i.e., C_{fn} and D_{fn}, must vanish in order that the stresses and the displacements be finite at r=0. Eq. (4) leads to a set of linear simultaneous equations by which the coefficients for the matrix region A_{mn}, B_{mn}, C_{mn}, D_{mn} are expressed in terms of the coefficients for the fiber region A_{fn}, B_{fn}. Similarly, the coefficients, A_{m0} and D_{m0}, are related to A_{f0}. The coefficients A_{f0}, A_{fn}, and B_{fn} are determined by satisfying the external boundary conditions.

The micromechanics problem of an interphase layer between the fiber and the matrix can also be analyzed using the present analysis technique by satisfying Eq. (4) at the

fiber/interphase and the interphase/matrix interfaces. The additional equations will be used to determine the unknown coefficients in the interphase region.

External Boundary Conditions

The displacement and stress conditions on the sides AB and BC (see Fig. 1(a)) for the square array and side EG for the diamond array constitute the external boundary conditions. For a given set of average strains ε_{x0} , ε_{y0}, and ε_{z0}, the following boundary conditions were presented in Ref. 9:

For the square array, along lines AB and BC:

$$\begin{aligned} &\theta = 0 \rightarrow \pi/4 \ : \qquad u|_{\theta} = \varepsilon_{x0} b, \quad \tau_{xy}\big|_{\theta} = 0, \\ &\theta = \pi/4 \rightarrow \pi/2 \ : \qquad v|_{\theta} = \varepsilon_{y0} b, \quad \tau_{xy}\big|_{\theta} = 0. \end{aligned} \tag{5}$$

Boundary conditions for the diamond array were determined by considering displacements and stresses for the diamond shaped region below the line EG (subscript 1) and for the diamond shaped region above line EG (subscript 2). Along line EG we have:

$$\begin{aligned} \theta_1 = 0 \rightarrow \pi/4 \ : \qquad u_1|_{\theta_1} = u_2|_{\phi_2} &= u_1|_{\phi_2} + \varepsilon_{x0}\sqrt{2}b, \\ &= -u_1|_{\theta_2} + \varepsilon_{x0}\sqrt{2}b, \\ &= -u_1\big|_{\frac{\pi}{2}-\theta_1} + \varepsilon_{x0}\sqrt{2}b. \end{aligned} \tag{6}$$

and,

$$\begin{aligned} \theta_1 = 0 \rightarrow \pi/4 \ : \qquad v_1|_{\theta_1} &= -v_1\big|_{\frac{\pi}{2}-\theta_1} + \varepsilon_{y0}\sqrt{2}b, \\ \sigma_{\eta}|_{\theta_1} &= \sigma_{\eta}\big|_{\frac{\pi}{2}-\theta_1}, \\ \tau_{\eta\varsigma}|_{\theta_1} &= \tau_{\eta\varsigma}\big|_{\frac{\pi}{2}-\theta_1}. \end{aligned} \tag{7}$$

The $\eta - \zeta$ axes are shown in Fig. 1(b) and are oriented at 45 degrees to the x-y axes. After substituting appropriately for the stresses and displacements in Eqs. (6) and (7) and using Eq. (4), the external boundary conditions can be expressed in terms of the coefficients A_{f0}, A_{fn} and B_{fn}. A simple point matching technique was used in which these conditions were satisfied at discrete points on the boundary. The Fourier series in Eq. (2) must, therefore, be truncated so that the number of terms, i.e., the number of arbitrary constants A_{fo}, A_{fn} and B_{fn} matches the number of independent boundary conditions satisfied at discrete points. These boundary conditions lead to a set of linear simultaneous equations by which A_{f0}, A_{fn} and B_{fn} are determined. For the present analysis, the boundary was divided into 5 degree segments. As a result, 37 terms in the Fourier series, i.e., 37 unknown constants were used for both the square and diamond arrays. It was shown in Ref. 8 that 37 terms were adequate for convergence of the results. In the present study, to check the accuracy of the analytical solutions, FM interface stress results were compared with finite element results for each loading case. These results will be described later. After the constants A_{f0}, A_{fn}, and B_{fn} are determined, the stress state in the unit cell is known for a given set of average strains ε_{x0} , ε_{y0}, and ε_{z0}. The FM interface stresses can then be calculated from the constants in the fiber region as

$$
\begin{aligned}
(\sigma_r)_i &= 2A_{f0} + \sum_{n=2,\ even}^{36} \left\{ \left(2 + n - n^2\right) a^n A_{fn} + \left(n - n^2\right) a^{n-2} B_{fn} \right\} \cos n\theta \\
(\tau_{r\theta})_i &= \sum_{n=2,\ even}^{36} n \left\{ (1 + n)\, a^n A_{fn} + (n - 1)\, a^{n-2} B_{fn} \right\} \sin n\theta
\end{aligned}
\tag{8}
$$

Calculation of Average Stresses

The average stresses due to applied strains on the unit cell are calculated simply by integrating over the appropriate region. For the square array,

$$\bar{\sigma}_x = \frac{1}{b}\int_0^b \sigma_x|_{x=0}\,dy = \frac{1}{b}\int_0^b \sigma_\theta|_{\theta=\pi/2}\,dr$$

$$\bar{\sigma}_y = \frac{1}{b}\int_0^b \sigma_y|_{y=0}\,dx = \frac{1}{b}\int_0^b \sigma_\theta|_{\theta=0}\,dr \qquad (9)$$

$$\bar{\sigma}_z = \frac{1}{b^2}\iint_{ABCD} \sigma_z\,dS = \frac{1}{b^2}\iint_{ABCD} [E_z\varepsilon_{z0} + \nu_{zr}(\sigma_r + \sigma_\theta)]\,dS$$

where ε_{z0} is the constant strain in the z-direction and ν_{zr} is the Poisson's ratio. All integrations were carried out exactly except for the $(\sigma_r + \sigma_\theta)$ term in the last equation, which was integrated numerically (over the matrix region) using Gauss quadrature. For the diamond array the same equations can be used if all the b terms in Eq. (9) are replaced by $\sqrt{2}b$ in the equations for $\bar{\sigma}_x$ and $\bar{\sigma}_y$ and ABCD is replaced by EGH in the equation for $\bar{\sigma}_z$.

Loading Procedures

The procedures for applying appropriate boundary conditions to achieve the different symmetric and anti-symmetric loading conditions and preserve the compatibility of the unit cell with its neighbors were developed in the present study and are presented in the following section.

Symmetric Loading Cases

Symmetric loads such as thermal, longitudinal, and transverse can be applied by imposing average strains ε_{x0} , ε_{y0}, and ε_{z0} appropriately. For the thermal loading case, the FM interface stresses were determined by a two step procedure. First, overall coefficients of thermal expansion for the composite were calculated using the macroscopic constitutive relation for the normal components of stress and strain.

$$\begin{Bmatrix} \varepsilon_{x0} \\ \varepsilon_{y0} \\ \varepsilon_{z0} \end{Bmatrix} = \begin{bmatrix} S_{11} & S_{12} & S_{13} \\ S_{12} & S_{22} & S_{23} \\ S_{13} & S_{23} & S_{33} \end{bmatrix} \begin{Bmatrix} \bar{\sigma}_x \\ \bar{\sigma}_y \\ \bar{\sigma}_z \end{Bmatrix} + \begin{Bmatrix} \alpha_x \Delta T \\ \alpha_y \Delta T \\ \alpha_z \Delta T \end{Bmatrix} \tag{10}$$

For a given ΔT and $\varepsilon_{x0} = \varepsilon_{y0} = \varepsilon_{z0} = 0$ imposed on the analysis model the overall α_x, for example, can then be computed using the relation,

$$\alpha_x = -(S_{11}\bar{\sigma}_x + S_{12}\bar{\sigma}_y + S_{13}\bar{\sigma}_z)/\Delta T \tag{11}$$

where $\bar{\sigma}_x$, $\bar{\sigma}_y$ and $\bar{\sigma}_z$ are the average stresses calculated using Eq. (9). The compliances S_{ij} in Eqs. (10) and (11) were calculated using only mechanical loading as described later. A similar procedure can be used to calculate overall α_y and α_z.

Next, FM interface stresses were calculated by imposing the overall strains $\varepsilon_{x0} = \alpha_x \Delta T$, $\varepsilon_{y0} = \alpha_y \Delta T$ and $\varepsilon_{z0} = \alpha_z \Delta T$ on the analysis model. The computed average stresses ($\bar{\sigma}_x$, $\bar{\sigma}_y$, $\bar{\sigma}_z$) for this set of strains will be zero since they simulate unconstrained thermal loading. Such a procedure ensured compatibility between adjacent unit cells during thermal loading. Both the square and diamond arrays can be analyzed by this procedure. For the case of temperature dependent material properties, the same two-step procedure can be used at each increment of temperature (see Ref. 10).

Longitudinal loading was applied by imposing $\varepsilon_{z0} = 1$ and $\varepsilon_{x0} = \varepsilon_{y0} = -\nu_{31}\,\varepsilon_{z0}$. The macroscopic Poisson's ratio, ν_{31} of the composite is determined by first considering the macroscopic Hooke's law for normal stresses:

$$\begin{Bmatrix} \bar{\sigma}_x \\ \bar{\sigma}_y \\ \bar{\sigma}_z \end{Bmatrix} = \begin{bmatrix} C_{11} & C_{12} & C_{13} \\ C_{12} & C_{22} & C_{23} \\ C_{13} & C_{23} & C_{33} \end{bmatrix} \begin{Bmatrix} \varepsilon_{x0} \\ \varepsilon_{y0} \\ \varepsilon_{z0} \end{Bmatrix} \tag{12}$$

and calculating the constants C_{ij}. For example, C_{11}, C_{12}, and C_{13} can be determined by imposing $\varepsilon_{x0} = 1$ and $\varepsilon_{y0} = \varepsilon_{z0} = 0$ on the analysis model. Based on Eq. (12), we have $C_{11} = \bar{\sigma}_x$, $C_{12} = \bar{\sigma}_y$, and $C_{13} = \bar{\sigma}_z$, where $\bar{\sigma}_x$, $\bar{\sigma}_y$ and $\bar{\sigma}_z$ are the average stresses calculated using Eq. (9). Similarly, the constants C_{22} and C_{23} can be determined by imposing $\varepsilon_{y0} = 1$ and $\varepsilon_{x0} = \varepsilon_{z0} = 0$ and C_{33} can be calculated by imposing $\varepsilon_{z0} = 1$ and $\varepsilon_{x0} = \varepsilon_{y0} = 0$. The C_{ij} matrix in Eq. (12) is then inverted to give the compliance matrix, S_{ij}, for normal stresses (see Eq. (10)). The unknown ν_{31} is equal to $-S_{13}/S_{33}$. A similar procedure is used to calculate ν_{21} which is given by $-S_{12}/S_{22}$. The FM interface stresses under transverse loading were calculated by imposing $\varepsilon_{x0} = 1$ and $\varepsilon_{y0} = -\nu_{12}\,\varepsilon_{x0}$, $\varepsilon_{z0} = -\nu_{13}\,\varepsilon_{x0}$. These procedures are equally applicable to both the square and diamond arrays.

Anti-symmetric Loading Cases

The inplane shear ($\bar{\tau}_{xy}$) and longitudinal shear ($\bar{\tau}_{yz}$) loading cases involve somewhat different considerations than the symmetric loading cases. Note that the square and the diamond arrays are essentially the same except for a 45 degree rotation. This fact can be used to advantage in the solution of these anti-symmetric loading cases.

***Inplane Shear Loading*:** Using the inplane strain transformation equations for a 45 degree rotation, applied normal strains $\varepsilon_{x0} = -1/2$ and $\varepsilon_{y0} = 1/2$ ($\gamma_{xy0} = \varepsilon_{z0} = 0$) on a square array model are equivalent to applied shear strains $\gamma_{xy0} = 1$ ($\varepsilon_{x0} = \varepsilon_{y0} = 0$) on a diamond array model. Similarly, applied normal strains $\varepsilon_{x0} = 1/2$ and $\varepsilon_{y0} = -1/2$ ($\gamma_{xy0} = \varepsilon_{z0} = 0$) on a diamond array model are equivalent to applied shear strains $\gamma_{xy0} = 1$ ($\varepsilon_{x0} = \varepsilon_{y0} = 0$) on a square array model. Thus, FM interface stresses under inplane shear loading for the square array model were obtained by imposing the appropriate normal strains on the diamond array model and using the same micromechanics analysis described earlier. Similarly, inplane shear loading for the diamond array model was analyzed using normal strains on the square array model.

***Longitudinal Shear Loading*:** The solution for the square array under longitudinal shear loading was presented in Ref. 9 for computing overall longitudinal shear stiffness. FM

interface stresses for the square array were calculated in the present study by using similar solution techniques. The solution for the diamond array under longitudinal shear loading could be obtained by imposing appropriate boundary conditions on the model as presented in Ref. 11. However, in the present study a simple procedure was developed to calculate FM interface stresses for this case. Once again the similarity of the square and the diamond arrays can be used to advantage in this case. If the FM interface stresses under longitudinal shear loading can be obtained for the square array, they can be obtained for the diamond array by simple transformations.

The governing equation for the square array under longitudinal shear loading can be written in terms of the longitudinal displacement w as [9]

$$\nabla^2 w = 0, \quad \nabla^2 = \frac{\partial^2}{\partial r^2} + \frac{1}{r}\frac{\partial}{\partial r} + \frac{1}{r^2}\frac{\partial^2}{\partial \theta^2} \tag{13}$$

The solution to this equation is obtained for an average applied shear strain γ_{yz0} (or γ_{xz0}). From the symmetry and anti-symmetry conditions, a general solution to Eq. (13) takes the form [9]

$$w = \sum_{n=1,\,odd}^{\infty} (A_n' r^n + B_n' r^{-n}) \sin n\theta, \tag{14}$$

where A_n' and B_n' are arbitrary constants that are determined by the internal and external boundary conditions. Internal boundary conditions at the fiber-matrix interface are given by

$$w_f = w_m, \quad (\tau_{rz})_f = (\tau_{rz})_m, \tag{15}$$

where f and m correspond to the fiber and matrix, respectively. Eq. (15) leads to a set of simultaneous equations by which A'_{mn} and B'_{mn} are expressed in terms of A'_{fn}. External boundary conditions on the sides AB and BC of the square array (Fig. 1(a)) can be written as

$$\begin{aligned} \theta = 0 \rightarrow \pi/4 \; : \quad & \frac{\partial w_m}{\partial x} = 0, \\ \theta = \pi/4 \rightarrow \pi/2 \; : \quad & w_m = b\,\gamma_{yz0}. \end{aligned} \tag{16}$$

These boundary conditions are satisfied at discrete points on the boundary to determine A'_{fn}. As shown in Ref. [9], using point matching for points at every 5 degree increment along the boundary was sufficient to achieve convergence of the numerical results. Once the constants A'_{fn} are determined, FM interface stresses can be computed as,

$$(\tau_{rz})_i = G^f_{rz} \sum_{n=1,\,odd}^{19} \{n\, a^{n-1} A'_{fn}\} \sin n\theta \tag{17}$$

where G^f_{rz} is the longitudinal shear modulus of the fiber and a is the fiber radius. The average applied stress on the model can be computed, after the arbitrary constants are determined, as

$$\bar{\tau}_{yz} = \frac{1}{b^2} \iint_{ABCD} \tau_{yz} dS. \tag{18}$$

A similar procedure can be used for an average applied shear strain γ_{xz0}.

The solution for the diamond array under longitudinal shear loading can be obtained from the solution of the square array by recalling that both arrays are essentially the same except for a rotation of 45 degrees. Using stress transformation equations for a 45 degree

rotation, an average shear stress $\bar{\tau}_{yz}$ applied to the diamond array is equivalent to applying equal longitudinal shear stresses $\bar{\tau}'_{xz}$ and $\bar{\tau}'_{yz}$ to the square array, and the two cases are related by:

$$\bar{\tau}_{yz} = \left[\frac{1}{(\cos 45^0 + \sin 45^0)}\right] (\bar{\tau}'_{yz} + \bar{\tau}'_{xz}). \tag{19}$$

Thus, FM interface stresses for the square array under equal longitudinal shear loadings $\bar{\tau}'_{xz}$ and $\bar{\tau}'_{yz}$ can be superposed according to Eq. (19) to obtain the FM stresses for the diamond array under longitudinal shear loading $\bar{\tau}_{yz}$.

The FM interface stress results for all the symmetric and anti-symmetric loadings for the square array were compared with finite element results to check the accuracy of the analytical solutions.

Finite Element Analysis

The finite element mesh used in the present study is shown in Fig. 2. It consisted of one layer of isoparametric hexahedral elements. Three dimensional elements were used to facilitate the imposition of generalized plane strain. There were 526 nodes and 238 elements in the model and the analysis was performed using the MSC/NASTRAN code [13]. The dimensions of the fiber radius, a, and the unit cell side, b, were chosen to represent a fiber volume fraction of 0.625. A generalized plane strain condition (for the symmetric loading cases) was imposed by constraining the z-displacement, w, to be zero on the back face and imposing w=constant (using multi-point constraints [13]) on the front face. For the transverse shear case, the out-of-plane displacements, w, were constrained to be zero throughout the model. For the longitudinal shear loading case, the inplane u- and v-displacements were constrained to be zero throughout the model. The different loading conditions and the corresponding displacement boundary conditions are listed in Table 1. A convergence study

was performed to decide upon the mesh refinement, especially in the region near the FM interface.

RESULTS AND DISCUSSION

FM interface stresses were computed using the analytical and finite element models for thermal, longitudinal, transverse, inplane shear, and longitudinal shear loadings. All the results were obtained for a graphite/epoxy, AS4/3501-6, unidirectional composite. The constituent material properties used in the present study [14] are given in Table 2.

Fig. 3 shows the normalized FM interface stresses under unit thermal loading ($\Delta T = -1$). The analytical results for the square and the diamond arrays are shown by solid and dashed lines, respectively. The finite element results for the square array are shown by solid circular symbols. There is excellent agreement between the closed-form and finite element results. Both the peak radial, σ_r, and the peak transverse shear, $\tau_{r\theta}$, stresses for the square and diamond arrays were the same except for a shift of 45 degrees. To characterize FM interface strength and predict interface failures, these thermal residual stresses will need to be superimposed with FM interface stresses from the mechanical loading cases. The variations in the interface stresses are due to the presence of the neighboring fibers. The effects of uneven fiber spacing on thermal residual stresses in a unidirectional metal matrix composite were studied in Ref. 15, which showed that the effect of closely spaced fibers on FM interface stresses can be analyzed by considering a regular array with a larger fiber volume fraction.

Figure 4 shows FM interface stresses under longitudinal loading ($\bar{\sigma}_z$). Once again, there is excellent correlation between the closed-form and finite element results. The stress concentrations (peak stress/applied stress) at the FM interface for this loading are very small since there is no load transfer across the interface under longitudinal loading. The interface stresses are purely a result of Poisson's ratio effects and fiber interactions. As before, the stresses for the square and diamond arrays were the same except for a shift of 45 degrees.

Figure 5 shows FM interface stresses under transverse loading ($\bar{\sigma}_x$). Once again there is excellent agreement between the closed-form and finite element results. The radial stress concentration for the square array was about 1.35. This was 30% higher than the stress concentration for the diamond array. Thus, in a transversely loaded composite the regions in which the fibers are arranged in a square array would be more likely sites for FM interface failures. The regions where the fibers are packed closer together are likely to be even more critical, as will be shown later.

The FM interface stresses for transverse shear loading ($\bar{\tau}_{xy}$) are shown in Fig. 6. There is excellent agreement between the closed-form and finite element results. The radial stress concentration of 1.54 for the diamond array was 40% higher than that for the square array. In contrast, the stress concentration for $\tau_{r\theta}$ of 1.23 for the square array was 25% higher than that for the diamond array. Depending on the relative FM interface strength under normal and shear loads, the regions in a composite which resemble a square array or a diamond array could be candidate sites for FM failures.

Figure 7 shows the FM interface shear stress, τ_{rz}, under longitudinal shear loading ($\bar{\tau}_{yz}$). The results from the closed-form analysis and the finite element analysis were in excellent agreement. This loading produced the highest stress concentration factor of 1.88 for the square array. There was a 60% difference in the peak τ_{rz} for the square and the diamond arrays. Also, the location of this peak was shifted by 45 degrees. In a composite, the regions that resemble a square array will be most likely to experience FM interface failures under longitudinal shear loading.

The variation of the peak FM interface stresses with fiber volume fraction can be readily studied using the analytical solutions. The effect of variations in V_f on the FM interface stress concentrations can be used as an indicator of the effect of uneven fiber spacing on FM stress concentrations. For example, the effect of fibers being closer together than the assumed distance 2b (Fig. 1(a)) could be studied by considering higher V_f values. The stress concentration factors for the square array, under mechanical loading, are plotted as a function

of fiber volume fraction in Fig. 8. The stress concentration factors K_{rr}, $K_{r\theta}$, and K_{rz} denote the normalized peak σ_r under transverse loading, normalized peak $\tau_{r\theta}$ under transverse shear loading, and normalized peak τ_{rz} stress under longitudinal shear loading, respectively. The K_{rr} was least affected by V_f. The finite element results for $V_f = 0.625$ and 0.7 are also shown as a further validation of the closed-form results, especially for higher fiber volume fractions. For low fiber volume fractions ($V_f < 0.5$), there is virtually no effect on the stress concentration factors. Thus, FM interface stresses calculated using a simple composite cylinder model would be adequate for $V_f < 0.5$. However, for $V_f > 0.5$ the effects of fiber interactions on the FM interface stresses become more apparent. For example, there was a 22% increase in the $K_{r\theta}$ when V_f was increased from 0.625 to 0.75. The K_{rz} was the most sensitive to V_f. It increased by 28% when the V_f was increased from 0.625 to 0.75. These results for increases in V_f suggest that the effects of fibers being closely spaced are minimal for transverse loading but they can be high for the shear loading cases and need to be accounted for when considering these cases.

CONCLUDING REMARKS

Closed-form techniques for calculating fiber-matrix (FM) interface stresses were presented for a unidirectional composite under thermo-mechanical loadings using repeating square and diamond regular arrays. An Airy's stress function micromechanics approach from the literature, developed for calculating overall composite moduli, was extended in the present study to compute FM interface stresses for a unidirectional graphite/epoxy (AS4/3501-6) composite under thermal, longitudinal, transverse, transverse shear and longitudinal shear loadings. Comparisons with finite element results indicated excellent agreement of the FM interface stresses for the square array.

Under thermal and longitudinal loading, FM peak stresses were the same for the square and the diamond arrays. The square array led to higher stress concentrations under transverse normal and longitudinal shear loadings. Under transverse shear loading, the square array had

a higher shear stress concentration, whereas the diamond array had a higher radial stress concentration. Stress concentration factors under transverse shear and longitudinal shear loadings were very sensitive to fiber volume fraction. The present analysis provides a simple way to calculate accurate FM interface stresses for both the square and diamond array configurations.

The stress concentrations under various loading cases will be different when thermal residual stresses are included with the mechanical stresses. Within a composite laminate, there will usually be a combination of normal and shear loadings in each ply. The present analysis provides a simple way to calculate accurate elastic FM interface stresses for both the square and diamond array configurations under combined thermo-mechanical loadings.

REFERENCES

1. Drzal, L. T., Rich, M. J. and Subramoney, S.: "Fiber-Matrix Bonding and its Effect on Composite Properties," *Proc. Third Ann. Conf., Adv. Comp. III, ASM International,* Detroit, MI, Sept. 15-17, 1987, pp. 305-308.
2. Chamis, C. C. and Sendeckyj, G. P.: "Critique on Theories Predicting Thermoelastic Properties of Fibrous Composites," *J. Comp. Mater.*, Vol. 2, July 1968, pp. 332-358.
3. Hashin, Z. and Rosen, W. B.: "The Elastic Moduli of Fiber-Reinforced Materials," *J. Appl. Mech.*, June 1964, pp. 223-232. Errata, March 1965, p. 219.
4. Foye, R. L.: "An Evaluation of Various Engineering Estimates of the Transverse Properties of Unidirectional Composites," *Proc. 10th Nat. Symp., Soc. Aerosp. Mater. Process Eng.*, San Diego, Calif., Nov. 9-11, 1966, pp. G-31 to G-42.
5. Adams, D. F. and Doner, D. R.: "Transverse Normal Loading of a Unidirectional Composite," *J. Comp. Mater.*, Vol. 1, Apr. 1967, pp. 152-164.
6. Adams, D. F. and Crane, D. A.: "Finite Element Micromechanical Analysis of a Unidirectional Composite Including Longitudinal Shear Loading," *Comp. Struct.*, Vol. 18, 1984, pp. 1153-1165.
7. Achenbach, J. D. and Zhu, H.: "Effect of Interphases on Micro and Macromechanical Behavior of Hexagonal-Array Fiber Composites," *J. Appl. Mech*, Vol. 57, 1990, pp. 956-963.
8. Kobayashi, S. and Ishikawa, T.: "Elastic Properties of Unidirectional Fiber-Reinforced Composites," *Fukugo Zairyo Kenkyu (Composite Materials and Structures)*, Vol. 3, No. 3, 1974, pp. 12-20.
9. Ishikawa, T. and Kobayashi, S.: "Elastic Properties of Unidirectional Fiber-Reinforced Composites II," *Fukugo Zairyo Kenkyu (Composite Materials and Structures)*, Vol. 3, No. 4, 1974, pp. 23-31.
10. Ishikawa, T., Koyama, K. and Kobayashi, S.: "Thermal Expansion Coefficients of Unidirectional Composites," *J. Comp. Mater.*, Vol. 12, April 1978, pp. 153-168.

11. Averill, R. C. and Carmen, G. P.: "Analytical Modeling of Micromechanical Stress Variations in Continuous Fiber-Reinforced Composites," *Proc. IUTAM (Int. Union of Theo. and Appl. Mech) Local Mechanics Concepts for Composite Materials*, Oct. 28-31, 1991.

12. Jones, R. M.: *Mechanics of Composite Materials*, Scripta Book Company (McGraw-Hill), Washington, D. C., 1975.

13. MSC/NASTRAN User's Manual, Vols. 1 and 2, Nov. 1989. The MacNeal-Schwendler Corporation, Los Angeles, California.

14. Adams, D. F. and Schaffer, B. G.: "Analytical/Experimental Correlations of Stiffness Properties of Unidirectional Composites," *Comp. Tech. Rev.*, Vol. 4, No. 2, Summer 1982, pp. 45-48.

15. Bigelow, C. A.: "The Effects of Uneven Fiber Spacing on the Thermal Residual Stresses in a Unidirectional SCS-6/Ti-15-3 Laminate," NASA TM 104225, Feb. 1992, National Aeronautics and Space Administration, Hampton, Virginia.

Table 1 -- Displacement boundary conditions applied to finite element model.

Loading	Boundary condition at x = b	y = b	x = 0	y = 0
Thermal, ΔT [a]	u=const.[b]	v=const.[b]	u=0	v=0
Longitudinal, $\bar{\sigma}_z$ [c]	u=const.[b]	v=const.[b]	u=0	v=0
Transverse, $\bar{\sigma}_x$	$u = \varepsilon_{x0}\, b$	v=const.[b]	u=0	v=0
Transverse shear, $\bar{\tau}_{xy}$	$v = \gamma_{xy0}\, b/2$	$u = \gamma_{xy0}\, b/2$	v=0	u=0
Longitudinal shear, $\bar{\tau}_{yz}$	u=v=0	$w = \gamma_{yz0}\, b$	u=v=0	w=0

[a]Thermal load was applied by imposing ΔT = constant at all nodes in the model.
[b]A constant displacement was achieved by imposing multi-point constraints on the indicated nodal displacements.
[c]Longitudinal loading was achieved by imposing $w = \varepsilon_{z0}\, t$ on the front face, where t was the thickness of the model.

Table 2 -- Material properties of the constituents [14].

Material	E_z (GPa)	E_r (GPa)	G_{zr} (GPa)	G_{rr} (GPa)	ν_{zr}	ν_{rr}	α_z (10^{-6}/°C)	α_r
Fiber (AS4)	220	13.8	34.0	5.5	0.20	0.25	-0.36	18.0
Matrix (3501-6)	4.3	4.3	1.6	1.6	0.34	0.34	40.00	40.0

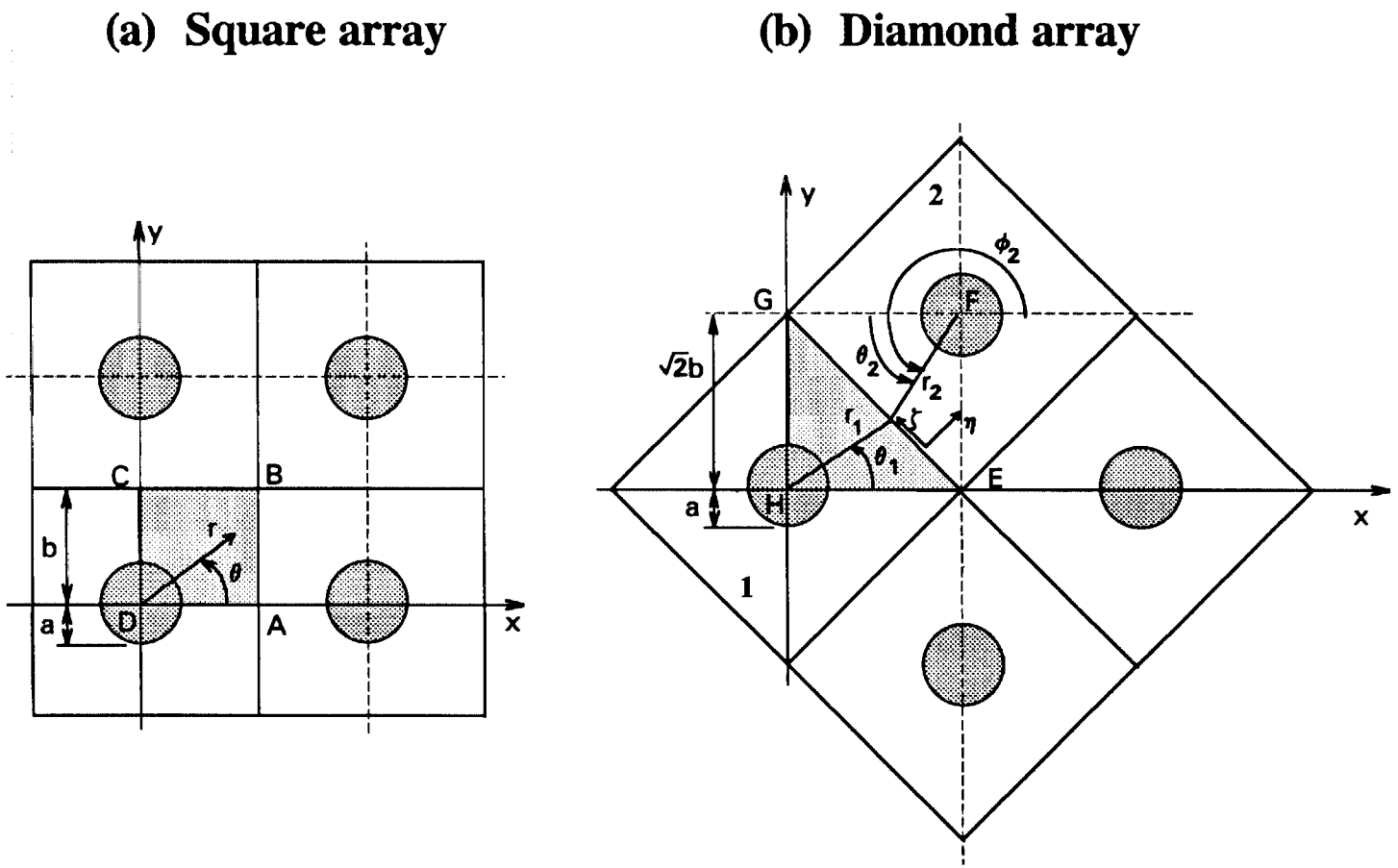

Figure 1. - Schematic of square and diamond array repeating unit cell configurations.

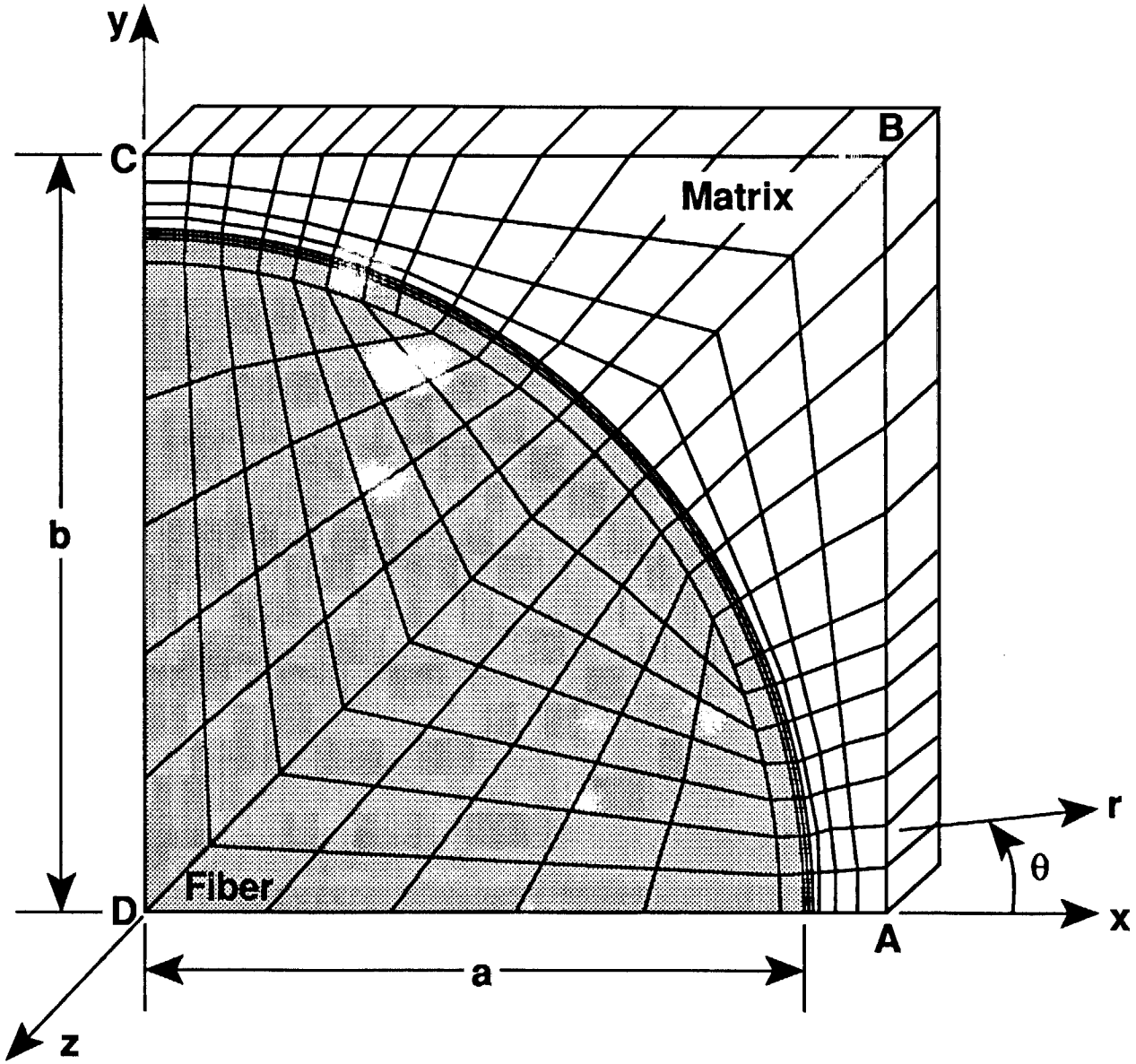

Figure 2. - Finite element model, $V_f = 0.625$.

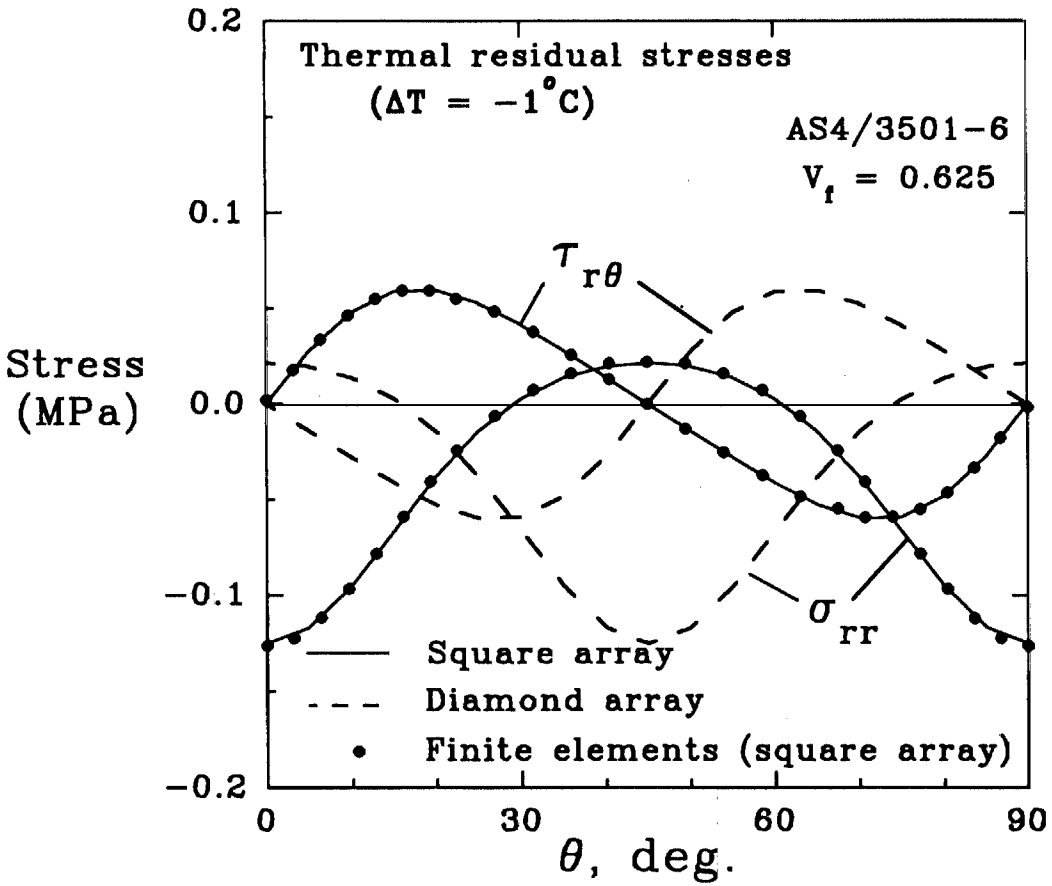

Figure 3. - FM interface stresses under unit thermal loading.

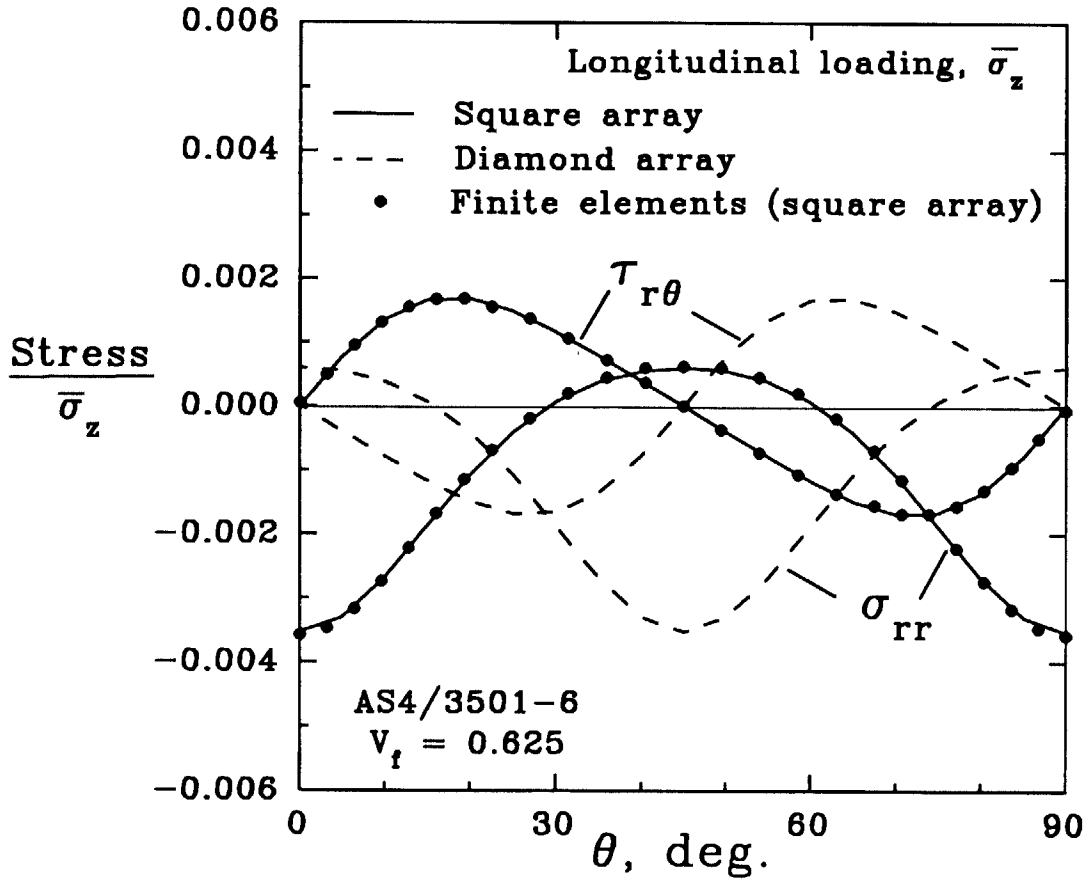

Figure 4. - Normalized FM interface stresses under longitudinal loading.

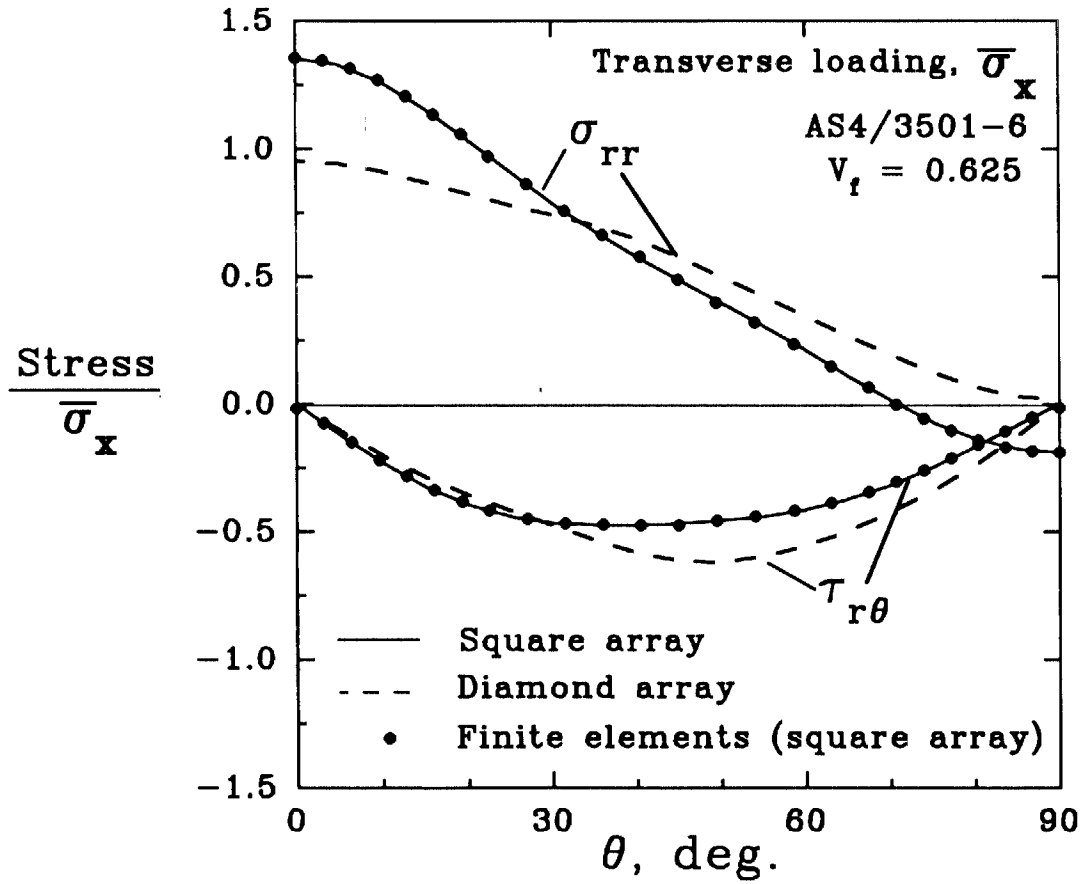

Figure 5. - Normalized FM interface stresses under transverse loading.

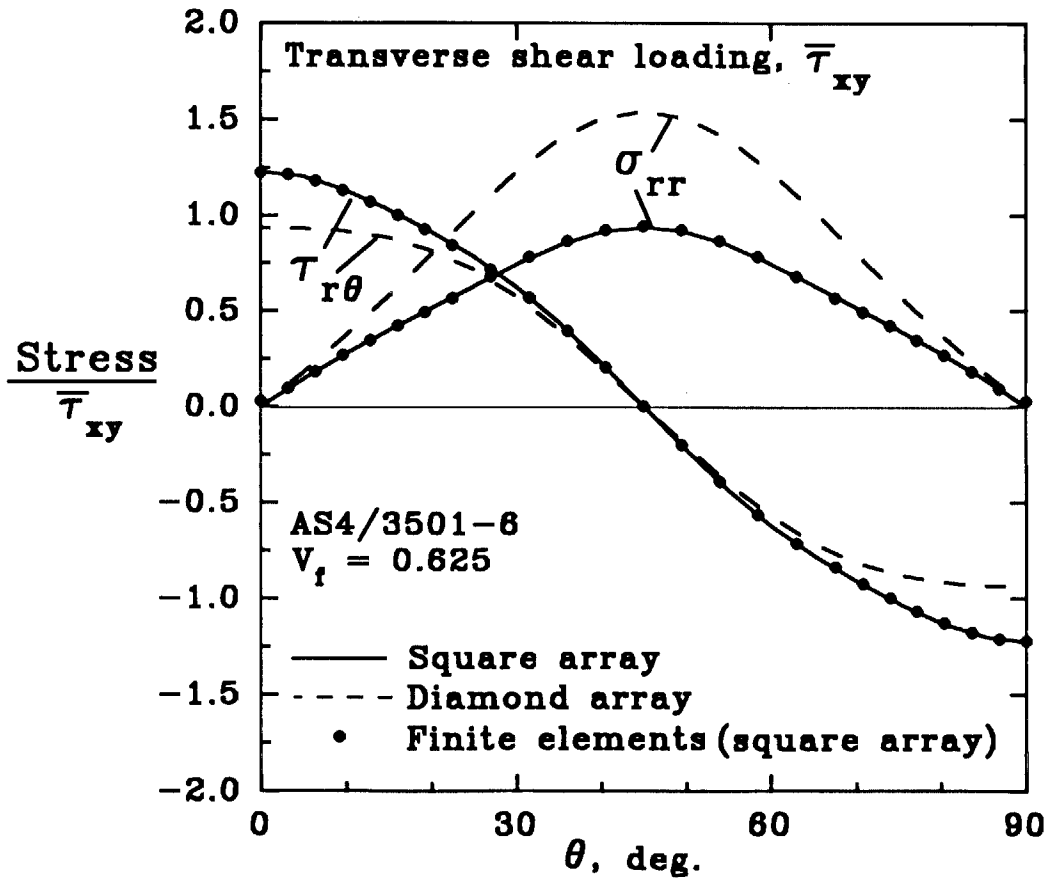

Figure 6. - Normalized FM interface stresses under transverse shear loading.

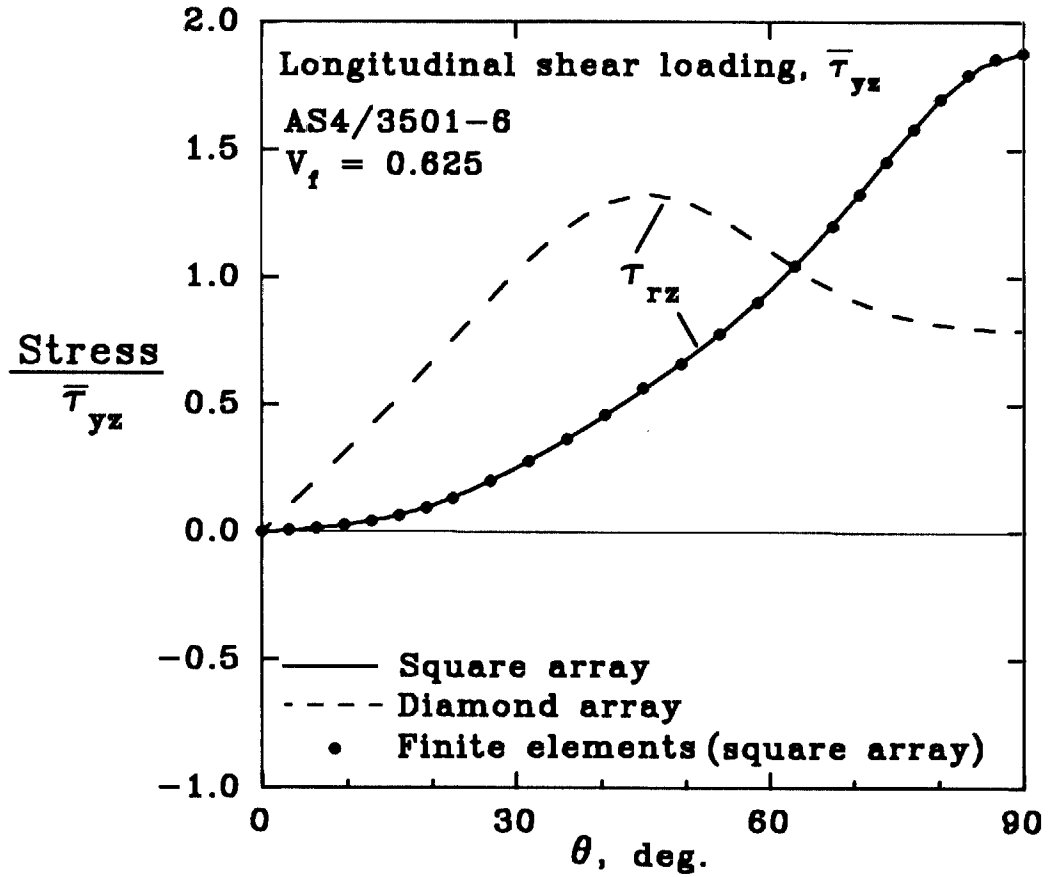

Figure 7. - Normalized FM interface stresses under longitudinal shear loading.

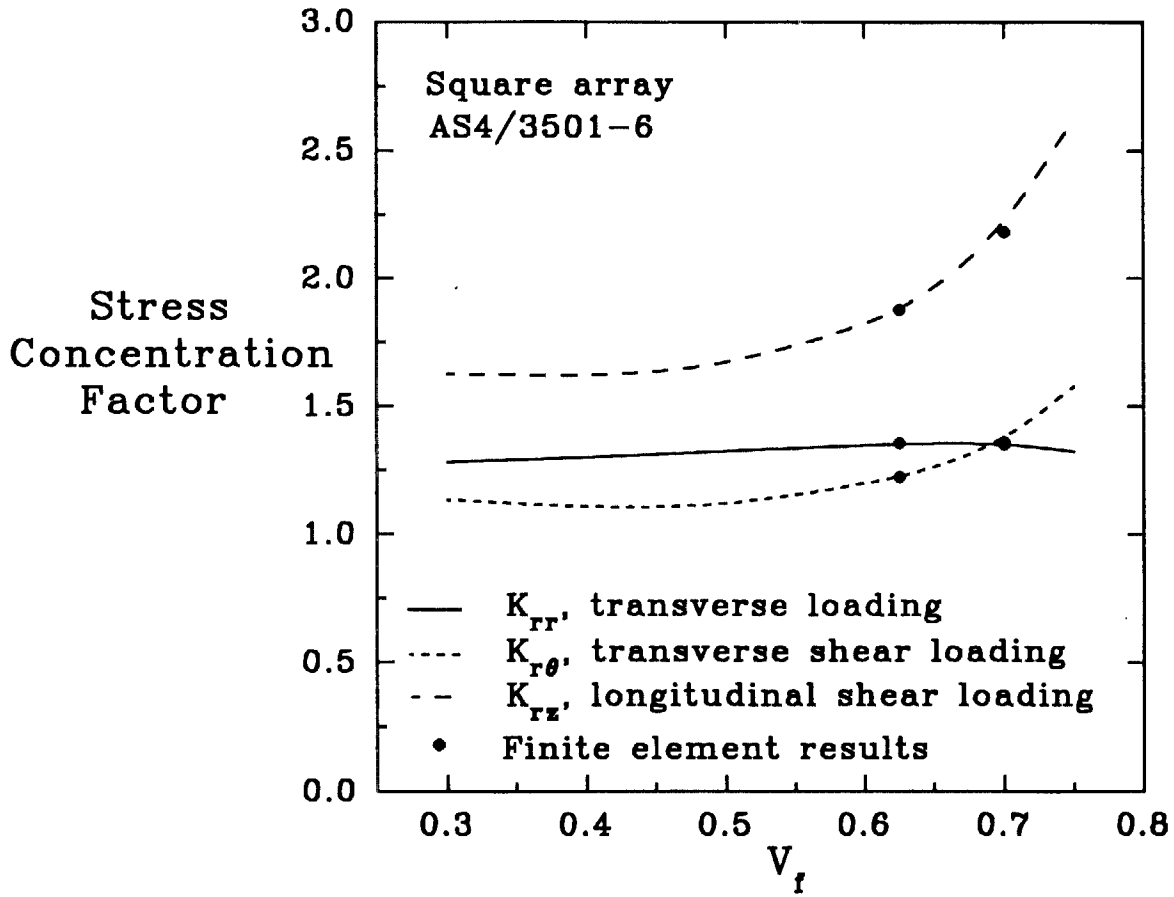

Figure 8. - FM interface stress concentration factors.

REPORT DOCUMENTATION PAGE

Form Approved
OMB No. 0704-0188

1. AGENCY USE ONLY *(Leave blank)*	2. REPORT DATE	3. REPORT TYPE AND DATES COVERED
	March 1992	Technical Memorandum

4. TITLE AND SUBTITLE

Closed-Form Analysis of Fiber-Matrix Interface Stresses Under Thermo-Mechanical Loadings

5. FUNDING NUMBERS

WU-505-63-50

6. AUTHOR(S)

Rajiv A. Naik and John H. Crews, Jr.

7. PERFORMING ORGANIZATION NAME(S) AND ADDRESS(ES)

NASA Langley Research Center
Hampton, VA 23665-5225

8. PERFORMING ORGANIZATION REPORT NUMBER

9. SPONSORING/MONITORING AGENCY NAME(S) AND ADDRESS(ES)

National Aeronautics and Space Administration
Washington, DC 20546

10. SPONSORING/MONITORING AGENCY REPORT NUMBER

NASA TM-107575

11. SUPPLEMENTARY NOTES

Naik: Analytical Services and Materials, Inc., Hampton, VA; Crews: Langley Research Center, Hampton, VA

12a. DISTRIBUTION/AVAILABILITY STATEMENT

Unclassified - Unlimited

Subject Category 39

12b. DISTRIBUTION CODE

13. ABSTRACT *(Maximum 200 words)*

Closed-form techniques for calculating fiber-matrix (FM) interface stresses, using repeating square and diamond regular arrays, were presented for a unidirectional composite under thermo-mechanical loadings. An Airy's stress function micromechanics approach from the literature, developed for calculating overall composite moduli, was extended in the present study to compute FM interface stresses for a unidirectional graphite/epoxy (AS4/3501-6) composite under thermal, longitudinal, transverse, transverse shear and longitudinal shear loadings. Comparisons with finite element results indicated excellent agreement of the FM interface stresses for the square array. Under thermal and longitudinal loading, the square array had the same FM peak stresses as the diamond array. The square array predicted higher stress concentrations under transverse normal and longitudinal shear loadings than the diamond array. Under transverse shear loading, the square array had a higher shear stress concentration while the diamond array had a higher radial stress concentration. Stress concentration factors under transverse shear and longitudinal shear loadings were very sensitive to fiber volume fraction. The present analysis provides a simple way to calculate accurate FM interface stresses for both the square and diamond array configurations.

14. SUBJECT TERMS

Repeating unit cell; Square array; Diamond array; Micromechanics; Composite

15. NUMBER OF PAGES

32

16. PRICE CODE

A03

17. SECURITY CLASSIFICATION OF REPORT	18. SECURITY CLASSIFICATION OF THIS PAGE	19. SECURITY CLASSIFICATION OF ABSTRACT	20. LIMITATION OF ABSTRACT
Unclassified	Unclassified		